Stochastic dynamics of two-dimensional particle motion in Darcy-scale heterogeneous porous media

Aronne Dell'Oca[1] **and Marco Dentz**[2]

[1]Dipartimento di Ingegneria Civile e Ambientale (DICA), Politecnico di Milano, Milan, Italy

[2]Spanish National Research Council (IDAEA-CSIC), Barcelona, Spain

Key Points:

- Flow topology determines transverse particle motion
- Transverse motion follows correlated Brownian motion
- Stochastic time-domain random walk model captures full two-dimensional particle transport

Corresponding author: Aronne Dell'Oca, aronne.delloca@polimi.it

Abstract

We study the upscaling and prediction of dispersion in two-dimensional heterogeneous porous media with focus on transverse dispersion. To this end, we study the stochastic dynamics of the motion of advective particles that move along the streamlines of the heterogeneous flow field. While longitudinal dispersion may evolve super-linearly with time, transverse dispersion is characterized by ultraslow diffusion, that is, the transverse displacement variance grows asymptotically with the logarithm of time. This remarkable behavior is linked to the solenoidal character of the flow field, which needs to be accounted for in stochastic models for the two-dimensional particle motion. We analyze particle velocities and orientations through equidistant sampling along the particle trajectories obtained from direct numerical simulations. This sampling strategy respects the flow structure, which is organized on a characteristic length scale. Perturbation theory shows that the longitudinal particle motion is determined by the variability of travel times, while the transverse motion is governed by the fluctuations of the space increments. The latter turns out to be strongly anti-correlated with a correlation structure that leads to ultraslow diffusion. Based on this analysis, we derive a stochastic model that combines a correlated Gaussian noise for the transverse motion with a spatial Markov model for the particle speeds. The model results are contrasted with detailed numerical simulations in two-dimensional heterogeneous porous media of different heterogeneity variance.

Plain Language Summary

The hydraulic conductivity of environmental geological formation can exhibit strong spatial variations. This leads to the formation of complex flow fields, whereas the flow tends to by-pass low conductivity areas and focuses within preferential flow paths. This complexity controls the transport dynamics of dissolved chemicals. Moreover, the hidden nature of the subsurface environment leads to a lack of knowledge about the details of the formation properties requiring a stochastic approach for the prediction of the fate of transported solutes. We propose a stochastic model capable of capturing the salient features of large scale solute transport in two dimensional heterogeneous Darcy flow. We accomplish the latter by incorporating key physical transport mechanisms that occur in the direction aligned with and transverse to the preferential flow orientation.

1 Introduction

Non-Fickian solute transport, that is, non-linear scaling of dispersion, non-Gaussian concentration distributions, early and late solute arrivals, have been documented in heterogeneous porous and fractured media from the pore to the regional scale (Berkowitz et al., 2006; Neuman & Tartakovsky, 2009; Bijeljic et al., 2011). The quantitative understanding of these behaviors plays a central role for the efficient modeling and prediction of large scale solute transport in environmental and industrial applications ranging from groundwater management and remediation (Domenico & Schwartz, 1998) to geological carbon dioxide storage (Niemi et al., 2017).

In the present work we focus on the transport of solute in two-dimensional Darcy-scale porous media that are characterized by spatial variability in the hydraulic conductivity. In this context, diffusion and mechanical dispersion control the dispersive character of solutes at the local scale, that is on lengths smaller than the characteristic heterogeneity length scale. At larger scales, solute dispersion is dominated by the heterogeneity of the hydraulic conductivity field, which underpins the emergence of complex flow fields. Large scale applications dealing with solute transport in geological media are concerned with scales on the order of ten to hundred times the characteristic correlation length of the hydraulic conductivity, at which the advective component of the motion is the prevailing factor controlling the dispersive behaviour of solutes (Rubin, 2003). Thus, we focus on purely advective transport, which provides the backbone for mixing and reaction processes (Dentz et al., 2022). We consider two-dimensional Darcy flows, which can represent flow in shallow aquifers, three dimensional formations characterized by a large correlation length in one spatial direction (e.g., stratification) (Rubin, 2003), as well as flow in rough fractures (Zimmerman & Bodvarsson, 1996; Z. Wang et al., 2020; Kottwitz et al., 2020; Kong & Chen, 2018; Hu et al., 2020). Furthermore, Lester et al. (2021, 2022) recently highlighted the profound similarity of the flow kinematics for Darcy flow in three-dimensional with those in two-dimensional heterogeneous porous media, which indicates that insights from two dimensions may be transferred to three-dimensional media.

The hidden nature of geological formations, in combination with spatial variations in their hydraulic properties, has led to the development of stochastic models to predict the fate of dissolved substances (Rubin, 2003; Neuman & Tartakovsky, 2009; Berkowitz

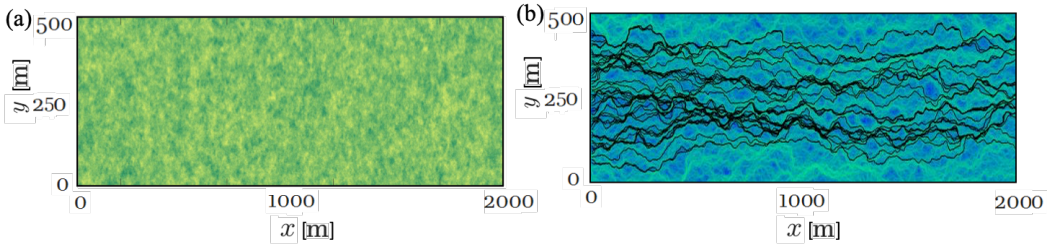

Figure 1: (Left panel)Spatial distribution of $Y(\mathbf{x})$ for $\sigma_Y^2 = 4$. (Right panel) Spatial organization of the module of the Darcy' velocity (logarithmic scale, blue low and green high) considering a strongly heterogeneous geological formation. Samples of particles trajectories are also drawn (black curves): note the emergence of preferential flow paths characterized by meandering-like structures as we proceed downstream from the injection location. The variance of the logarithm of $K(\mathbf{x})$ is 4, its correlation length is 10 m.

et al., 2006; Frippiat & Holeyman, 2008; Dell'Oca et al., 2018, 2019). In this context, major efforts have been devoted to conceptualize and formalize effective stochastic models to quantify average solute transport along the mean flow direction. These efforts include stochastic perturbation theory (Rubin, 2003), self-consistent time-domain random walk formulations (Cvetkovic et al., 2014; Fiori et al., 2015, 2013) through the use of fractional advection-diffusion equations (Benson et al. (2000); Y. Zhang et al. (2009)), multirate mass transfer approaches (Haggerty & Gorelick, 1995; Harvey & Gorelick, 2000), and continuous time random walks (Edery et al., 2014; Comolli et al., 2019; Dentz et al., 2020).

Transverse dispersion can be measured by the displacement variance of advectively transported solute particles (Dagan, 1989). Using stochastic perturbation theory, it has been shown (Dagan, 1984) that transverse dispersion grows ballistically at short times, that is with the square of time, and eventually crosses over to an ultra-slow dispersive behavior that is characterized by a growth with the logarithm of time. As a consequence, the transverse dispersion coefficient, which is defined in terms of the time-derivative of the displacement variance, decays to zero asymptotically. This is an exact result, which can be derived without recourse to perturbation theory (Attinger et al., 2004), and which has been observed in direct numerical simulations of flow and transport in two-dimensional heterogeneous porous media (Bellin et al., 1992; Salandin & Fiorotto, 1998; de Dreuzy

et al., 2007). This ultra-slow dispersion behavior is intimately linked to the meandering of the streamlines that arise because the flow field is divergence-free. The streamline meandering is illustrated in Figure 1, which shows a colormap of the flow speeds together with a set of purely advective particle trajectories. It is interesting to note that ultra-slow dispersion emerges in a variety of systems characterized by crowded or confined environments such as dense colloids (Boettcher & Sibani, 2011) and colloidal hard-sphere system, (Sperl, 2005), for vacancy-mediated diffusive motion, (Bénichou & Oshanin, 2002), and diffusion in a random force landscapes (Havlin & Ben-Avraham, 2002), but also in human mobility, (Song et al., 2010). In the context of flow in two-dimensional porous media, the confinement arises from the fact that the flow is divergence-free, which dictates the spatial organization of the streamlines.

The constraint imposed by the flow topology on transverse dispersion needs to be reflected in large scale transport models for streamwise and transverse solute dispersion. The multi-dimensional CTRW approach of Dentz et al. (2004) represents transverse dispersion in heterogeneous media through uncorrelated Gaussian-distributed space increments combined with random transition times. W. Wang & Barkai (2020) derive a two-dimensional fractional-in-space advection-dispersion equation based on this approach to represent the bulk dispersion behavior in geological media. These models do not account for the topological constraints imposed by the divergence-free Darcy flow equation. In fact, this type of CTRW represents particle motion under spatially random retardation properties (Dentz & Castro, 2009).

Meerschaert et al. (2001) proposed a multi-dimensional fractional diffusion model to capture super-diffusive anisotropic transport regimes along the longitudinal and the transverse directions. Y. Zhang & Benson (2013) use a two-dimensional space-time fractional approach with space-dependent diffusion coefficients to model the vertically integrated tritium plumes of the MADE-2 experiment. Also these frameworks do not account for the impact of topological constraints on transverse dispersion.

Meyer & Tchelepi (2010) propose a Langevin model for the evolution of streamwise and transverse particle velocities that uses drift and diffusion coefficients that are obtained by calibrating suitable continuous functions to Monte-Carlo simulations of the direct flow and transport problem. This formulation reproduces the evolution of longitudinal and transverse dispersion. The framework was used for uncertainty quantifica-

tion in subsurface flows (Meyer et al., 2013), and its relation to first-order perturbation theory was studied in view of the model parameterization (Meyer, 2017, 2018).

In this paper we study the stochastic dynamics of particle motion in two-dimensional Darcy flow with focus on the evolution of particle displacements transverse to the mean flow direction. To this end we study particle speeds and orientations sampled equidistantly along trajectories from detailed numerical flow and transport simulations. Based on this analysis and using exact analytical expressions for the autocorrelation function of the orientation angle, we propose a stochastic approach for the two-dimensional particle motion that explicitly accounts for the constraint imposed on transverse particle motion by the flow topology.

Section 2 poses the flow and transport problem in two-dimensional heterogeneous porous media, defines the target variables and describes the direct numerical simulations. Section 3 reports on the quantification of the stochastic particle motion using perturbation theory for weak heterogeneity and in terms of a stochastic time-domain random walk model for strong medium heterogeneity. Section 4 validates the derived two-dimensional model against detailed numerical simulations.

2 Flow and transport in heterogeneous porous media

In this section we provide the details about the heterogeneous spatial arrangement of the hydraulic conductivity field, and the Darcy scale flow and transport problem. Furthermore, we define the transport-related observables.

2.1 Darcy flow and hydraulic conductivity

Flow in porous media is described on the continuum scale by the Darcy equation (Bear, 1972)

$$\mathbf{q}(\mathbf{x}) = -K(\mathbf{x})\nabla h(\mathbf{x}), \tag{1}$$

where $\mathbf{x}$ denotes the two-dimensional space coordinate vector with components x and y, $\mathbf{q}$ is the Darcy flux vector (with components q_x and q_y) and $h(\mathbf{x})$ is the hydraulic head, The hydraulic conductivity $K(\mathbf{x})$ is a scalar. We do not consider sinks or sources and consider fluid and solid matrix as incompressible such that $\nabla \cdot \mathbf{q}(\mathbf{x}) = 0$.

In order to represent the spatial variability of the hydraulic conductivity we model $K(\mathbf{x})$ as a multi-Gaussian random field with lognormal marginal distribution (Rubin, 2003) and geometric mean K_G. That is, the log-hydraulic conductivity $Y(\mathbf{x}) = \ln[K(\mathbf{x})/K_G]$ is represented as a second-order stationary multi-Gaussian random field characterized by zero mean and the isotropic exponential covariance function

$$\langle Y(\mathbf{x})Y(\mathbf{x}')\rangle = \sigma_Y^2 \exp\left(-|\mathbf{x}-\mathbf{x}'|/\ell_Y\right), \tag{2}$$

where, σ_Y^2 and ℓ_Y are the variance and the correlation length of Y, respectively. The angular brackets denote the ensemble average. In the following all length are non-dimensionalized with ℓ_Y.

The mean hydraulic gradient is aligned with the x–direction of the coordinate system such that the mean Darcy velocity is $\langle q_i(\mathbf{x})\rangle = \delta_{i1}\overline{q}$. The Eulerian fluid velocity vector $\mathbf{v}(\mathbf{x})$ is obtained by rescaling the flux vector as $\mathbf{v}(\mathbf{x}) = \mathbf{q}(\mathbf{x})/\phi$, where ϕ is porosity. In the following, we assume that porosity is constant and set it equal to one, which is equivalent to rescaling time. The Eulerian mean velocity is $\langle v_i(\mathbf{x})\rangle = \delta_{i1}\overline{v}$. The characteristic advection time is defined by $\tau_v = \ell_Y/\overline{v}$.

The magnitude $v(\mathbf{x}) = |\mathbf{v}(\mathbf{x})|$ of the Eulerian velocity denotes the flow speed. The Eulerian flow field is characterized by the distribution $p_e(v)$. It is obtained by spatial sampling as

$$p_e(v) = \lim_{V\to\infty} \frac{1}{V} \int_\Omega d\mathbf{x}\delta[v - v_e(\mathbf{x})], \tag{3}$$

where Ω is the sampling domain and V its volume. Due to ergodicity, spatial sampling of v_e is equivalent to ensemble sampling, and thus, $p_e(v) = \langle\delta[v - v_e(\mathbf{x})]\rangle$. In the following, velocities and speeds are rescaled by $\overline{v}$. This implies that $\langle v_e\rangle = \chi$ is equal to the advective tortuosity (Comolli et al., 2019).

2.2 Particle motion

We focus on purely advective transport due to its relevance for large-scale scenarios. We adopt a Lagrangian perspective by considering solute particles of equal mass whose trajectories $\mathbf{x}(t)$ are given by

$$\frac{d\mathbf{x}(t)}{dt} = \mathbf{w}(t), \tag{4}$$

where $\mathbf{w}(t) = \mathbf{v}[\mathbf{x}(t)]$ is the isochronic Lagrangian speed and t is time. The initial particle position is denoted by $\mathbf{x}(t=0) = \mathbf{x}_0$.

The particle speed is given by $w(t) = |\mathbf{w}(t)|$. The point PDF $p_t(v)$ of $w(t)$ sampled over all streamlines is equal to the PDF $p_e(v)$ of Eulerian speeds (Hakoun et al., 2019)

$$p_t(v) = p_e(v). \tag{5}$$

This is a result of the fact that the flow is volume conserving. In the following, we consider a uniform initial distribution of particle positions across the cross-section of the medium. This implies that the distribution $p_0(v)$ of initial speeds $v_0 = w_0(t = 0) = v(\mathbf{x}_0)$ is $p_0(v) = p_e(v)$ is equal to $p_e(v)$. That is, the initial speeds distribution is equal to the steady state distribution.

For our analysis it is convenient to consider the advective particle motion as a function of the streamwise distance (Comolli et al., 2019)

$$\frac{d\hat{\mathbf{x}}(s)}{ds} = \frac{\mathbf{u}(s)}{u(s)}, \qquad \frac{dt(s)}{ds} = \frac{1}{u(s)}, \tag{6}$$

where s is the particle streamwise coordinate, $\mathbf{u}(s) = \mathbf{v}[\hat{\mathbf{x}}(s)]$ is the s-Lagrangian velocity and $u(s) = |\mathbf{u}(s)|$ is the s-Lagrangian speed. The point PDF $p_s(v)$ of $v_s(s)$ is equal to the flux-weighted Eulerian speed PDF (Hakoun et al., 2019)

$$p_s(v) = \frac{v p_e(v)}{\langle v_e \rangle}. \tag{7}$$

The distribution of initial speeds $v_s(s = 0) = v_0 = v_t(t = 0)$ is $p_e(v)$. This implies that the speed statistics evolve towards the steady state $p_s(v)$ with distance along the streamlines. The particle displacement in time is obtained in terms of $\hat{\mathbf{x}}(s)$ as $\mathbf{x}(t) = \hat{\mathbf{x}}[s(t)]$, where $s(t) = \max[s|t(s) \leq t]$.

Our goal is to upscale the motion of solute particles that are advected in a Darcy scale heterogeneous flow field. As descriptors of the stochastic motion of the solute particles, we consider the evolution of the dispersion scales along the longitudinal and the transverse directions, that is,

$$\sigma_x(t) = \sqrt{\langle [x(t) - \langle x(t) \rangle]^2 \rangle}, \qquad \sigma_y(t) = \sqrt{\langle y(t)^2 \rangle}. \tag{8}$$

Note that, along the transverse direction the average particle position is zero, that is, $\langle y(t) \rangle = 0$, due to the uniform in the mean flow conditions. The knowledge of the dispersive scales σ_x and σ_y can be insufficient to properly characterize solute transport in case the probability distribution of $x(t)$ and $y(t)$ are not Gaussian. Thus, we consider

also the probability distributions of the longitudinal and transverse particle positions centered to their respective mean, that is,

$$p(x,t) = \langle \delta(x - [x(t) - \langle x(t) \rangle]) \rangle, \qquad p(y,t) = \langle \delta[y - y(t)] \rangle. \tag{9}$$

Note that, we subtract the average longitudinal particles position $\langle x(t) \rangle$ for convenience. Finally, we also consider the joint probability density function for the longitudinal and transverse particle positions, that is,

$$p(\mathbf{x},t) = \langle \delta[\mathbf{x} - \mathbf{x}(t)] \rangle. \tag{10}$$

2.3 Numerical Simulations

We consider a two dimensional domain of size $600\ell_Y \times 150\ell_Y$. Different realizations of $Y(\mathbf{x})$ are generated using a sequential Gaussian simulator (Deutsch & Journel, 1992) on a regular Cartesian grid with element size equal to $\ell_Y/10$. We generate 100 Monte Carlo realizations of $Y(\mathbf{x})$ for three different scenarios with $\sigma_Y^2 = 1, 2$ and 4.

For the flow problem, we impose permeameter-like boundaries conditions, that is, no-flow along the bottom ($y = 0$) and top ($y = 150\ell_Y$) boundaries, a fixed value of the hydraulic head along the left ($x = 0$) boundary and $q_i = \delta_{ix}$ along the right ($x = 600\ell_Y$) boundary. Note that, the imposed boundary conditions lead to a uniform in the mean flow, $\langle q_i \rangle = \delta_{ix}$. Thus, we identify x as the longitudinal (or mean flow) direction and y as the transverse direction. We use the same grid structure employed for the generation of $Y(\mathbf{x})$. The flow problem is solved numerically using a mixed-finite element solver (Younes et al., 2010). The flow statistics are sampled over a subregion of $560\ell_Y \times 110\ell_Y$ to avoid boundary effects.

The numerical solution of the transport problem is based on the discretized version of (6),

$$\hat{\mathbf{x}}_{n+1} = \hat{\mathbf{x}}_n + \frac{\mathbf{v}_e(\hat{\mathbf{x}}_n)\Delta s}{|\mathbf{v}_e(\hat{\mathbf{x}}_n)|}, \qquad t_{n+1} = t_n + \frac{\Delta s}{|\mathbf{v}_e(\hat{\mathbf{x}}_n)|} \tag{11}$$

where $\hat{\mathbf{x}}_n = \hat{\mathbf{x}}(s_n)$, $t_n = t(s_n)$, $s_n = n\Delta s$ and Δs is the constant spatial increment here set to $\Delta s = \ell_Y/100$. We inject 110 particles uniformly spaced over a straight line perpendicular to the mean flow direction covering $90\ell_Y$. The line is placed at at distance of $30\ell_Y$ downstream from the $x = 0$ boundary and at distances of $20\ell_Y$ from the lateral boundaries. A bilinear interpolation scheme is used to determine the flow velocities within grid cells (Pollock, 1988).

3 Stochastic particle motion

In this section, we study the stochastic dynamics of two-dimensional particle motion in random Darcy' flow fields. In heterogeneous porous media, streamlines are tortuous as illustrated in Figure 1. Therefore, the velocity varies along the streamlines. The series $\{w(t)\}$ of isochronously sampled Lagrangian speeds typically exhibits intermittent behaviour, that is, long periods of low speeds alternate with short periods of intensively fluctuating high speeds (Hakoun et al., 2019). This intermittent behavior is due to the fact that flow velocities vary on a characteristic length scale, rather than a time scale. Therefore, the residence time in low velocities is higher than in high velocities. As a consequence, the equidistantly sampled velocity series $\{u(s)\}$ is not intermittent. Thus, we consider here particle motion as a function of streamline distance as expressed by Eqs. (6), that is, in terms of a time-domain random walk. In this context, we first recall results from second-order perturbation theory in the fluctuations of $\mathbf{v}(\mathbf{x})$ around its mean value, which is valid for low and moderate spatial heterogeneity. Then, we use a stochastic time-domain random walk approach to capture two-dimensional particle motion at higher degree of heterogeneity.

3.1 Perturbation theory

We expand the equations of motion (6) up to first order in the fluctuations of the random flow field $\mathbf{v}'(\mathbf{x}) = \mathbf{v}(\mathbf{x}) - \overline{\mathbf{v}}$. Thus, we obtain

$$\frac{d\hat{x}(s)}{ds} = 1, \qquad \frac{d\hat{y}(s)}{ds} = \frac{v_y[\hat{\mathbf{x}}_0(s)]}{\overline{v}}, \qquad \frac{dt(s)}{ds} = \frac{1}{\overline{v}} - \frac{v_x'[\hat{\mathbf{x}}_0(s)]}{\overline{v}^2}, \tag{12}$$

where $\hat{\mathbf{x}}_0(s) = (s, 0)^\top$. The superscript $\top$ denotes the transpose. Note that $v_y'(\mathbf{x}) = v_y(\mathbf{x})$. We consistently omit terms of quadratic order in the velocity fluctuations. From Eqs. (12), we obtain for $\hat{\mathbf{x}}(s)$

$$\hat{x}(s) = s, \qquad \hat{y}(s) = \int_0^s ds' v_y[\hat{\mathbf{x}}_0(s)] \tag{13}$$

The particle displacement $\mathbf{x}(t)$ in time is given by $\mathbf{x}(t) = \hat{\mathbf{x}}[s(t)]$. With $s(t) = \max[s|t(s) \leq t]$, the longitudinal displacement can be written as

$$x(t) = \max[s|t(s) \leq t] = \overline{v}t + \int_0^t dt' v_x'[\mathbf{x}_0(t')], \tag{14}$$

where $\mathbf{x}_0(t) = (\overline{v}t, 0)^\top$. This formulation shows that the longitudinal particle motion is determined by the variability of travel time $t(s)$. The transverse displacement is given

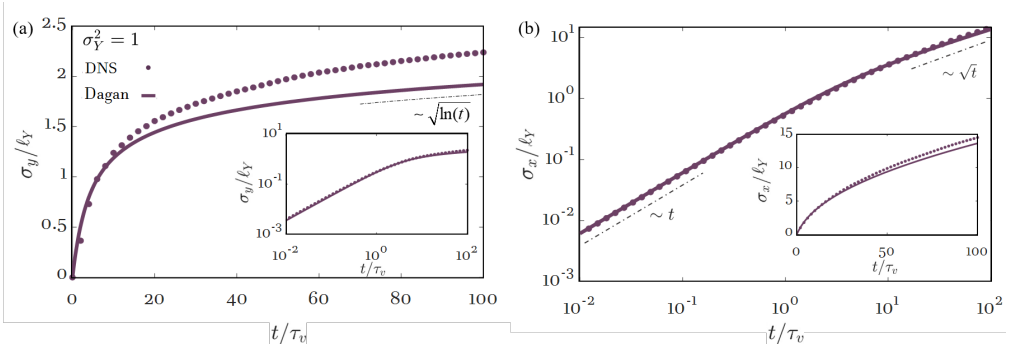

Figure 2: Time behaviour of (a) the transverse σ_y and (b) longitudinal dispersive scale σ_x considering results grounded on the direct numerical simulation (DNS - symbols) and the perturbation theory solution of Dagan, Eq. (22) and Eq. (30) (Dagan - solid curves), for a mildly degree of heterogeneity, i.e., $\sigma_Y^2 = 1$.

by

$$y(t) = \int_0^{\overline{v}t} ds' v_y[\mathbf{x}_0(s)] = \hat{y}(\overline{v}t). \tag{15}$$

It is determined by the variability of the spatial increment rather than the travel time.

3.1.0.1 Transverse dispersion We consider now the transverse increment process

$$\nu(s) = \sin[\alpha(s)] = \frac{v_y[\hat{\mathbf{x}}_0(s)]}{\overline{v}}, \tag{16}$$

where $\alpha(s)$ is the angle between the tangent of the streamline at distance s and the x-direction. In first-order perturbation theory, $\alpha(s) = \nu(s)$. That is, the statistic of $\nu(s)$ and $\alpha(s)$ are identical in this approximation. In order to determine their statistics, we first determine the statistics of $v_y(\mathbf{x})$. First-order perturbation theory in $Y(\mathbf{x})$ renders $v_y(\mathbf{x})$ as a linear functional of $Y(\mathbf{x})$ (Dagan, 1984),

$$v_y(\mathbf{x}) = \overline{v} \int_{-\infty}^{\infty} d\mathbf{x}' \kappa_y(\mathbf{x} - \mathbf{x}') Y(\mathbf{x}'). \tag{17}$$

The kernel $\kappa_y(\mathbf{x})$ can be written as

$$\kappa_y(\mathbf{x}) = \frac{\partial^2 G(\mathbf{x})}{\partial x \partial y}, \qquad G(\mathbf{x}) = -\frac{1}{2\pi} \ln(|\mathbf{x}|). \tag{18}$$

As $Y(\mathbf{x})$ is a Gaussian distributed random field, the linearity of relation (17) implies that $v_y(\mathbf{x})$ is also Gaussian distributed. Since $v_y(\mathbf{x})$ is a Gaussian random field, also $\nu(s)$ is Gaussian. Thus, they can be fully characterized by the mean, variance σ_ν^2 and correlation function $\rho_\nu(s) = \langle \nu(s'+s)\nu(s')\rangle/\sigma_\nu^2$. Its mean is $\langle \nu(s)\rangle = 0$, its variance is $\sigma_\nu^2 = \sigma_Y^2/8$ and its correlation function is $\rho_\nu(s) = f(s/\ell_Y)$ where (Hsu, 1999)

$$f(s) = \frac{72}{s^4} - \frac{4}{s^2} - 8\left(\frac{1}{s} + \frac{4}{s^2} + \frac{9}{s^3} + \frac{9}{s^4}\right)\exp(-s). \tag{19}$$

The increment process $\nu(s)$ is a stationary multi-Gaussian process. In other words, it is a correlated Gaussian noise. Thus, transverse particle motion describes the correlated random walk

$$\frac{d\hat{y}(s)}{ds} = \nu(s). \tag{20}$$

The mean transverse displacement is $\langle \hat{y}(s)\rangle = 0$, and its variance $\hat{\sigma}_y^2(s)$ is

$$\hat{\sigma}_y^2(s) = 2\sigma_\nu^2 \int_0^s ds' \int_0^{s'} ds'' \rho_\nu(s''). \tag{21}$$

The double integral can be evaluated explicitly by inserting expression (19), which gives (Dagan, 1988)

$$\hat{\sigma}_y^2(s) = \sigma_Y^2 \ell_Y^2 \left[\ln(s/\ell_Y) - \frac{3}{2} + \gamma + E_1(s/\ell_Y) + \frac{\ell_Y^2}{s^2} - \frac{3\ell_Y^2 \exp(-s/\ell_Y)(1+s/\ell_Y)}{s^2}\right]. \tag{22}$$

where γ is the Euler-Mascheroni constant and $E_1(t)$ the exponential integral (Abramowitz & Stegun, 1972). The displacement variance $\sigma_y^2(t)$ is obtained according to Eq. (15) by setting $s = \overline{v}t$ in Eq. (22). In the limit $s \ll 1$, Eq. (22) is quadratic in s,

$$\hat{\sigma}_y^2(s) = \sigma_\nu^2 s^2. \tag{23}$$

For distances $s \gg \ell_Y$, it evolves as

$$\hat{\sigma}_y^2(s) = \sigma_Y^2 \ell_Y^2 \ln(s/\ell_Y). \tag{24}$$

It grows with the logarithm of time, that is, it shows ultraslow diffusion, which is due to the transverse confinement of the streamlines of the flow field. Figure 2 shows the evolution of $\sigma_y(t)$ given by Eq. (22) for $s = \overline{v}t$. The perturbation theory expression is compared to direct numerical simulations for $\sigma_Y^2 = 1$. While the perturbation theory provides a good description of the overall evolution of $\sigma_y(t)$, it underestimates $\sigma_y(t)$ for times larger than τ_v. Nevertheless, the data confirms the predicted asymptotic $\ln(t)$ scaling of $\sigma_y^2(t)$.

3.1.0.2 Streamwise dispersion For completeness, we provide here also the perturbation theory results for streamwise dispersion. The streamwise velocity $v_x(\mathbf{x})$ is given in perturbation theory by (Dagan, 1984)

$$v'_x(\mathbf{x}) = \overline{v} \int_{-\infty}^{\infty} d\mathbf{x}' \kappa_x(\mathbf{x}-\mathbf{x}') Y(\mathbf{x}'), \tag{25}$$

where the kernel $\kappa_x(\mathbf{x})$ is defined by

$$\kappa_x(\mathbf{x}) = \delta(\mathbf{x}) - \frac{\partial^2 G(\mathbf{x})}{\partial x^2}. \tag{26}$$

Thus, $v_x(\mathbf{x})$ is a correlated Gaussian random field. As a consquence, the Lagrangian velocity fluctuation $w'_x(t) \equiv v_x[\mathbf{x}_0(t)]$ is a correlated Gaussian process and $x(t)$ satisfies the correlated random walk

$$\frac{dx(t)}{dt} = \overline{v} + w'_x(t). \tag{27}$$

The mean of $w'_x(t)$ is zero and its variance is given by $\sigma^2_{w_x} = 3\overline{v}^2\sigma^2_Y/8$. Its correlation function is $\rho_{w_x}(t) = g(t/\tau_v)$ with (Hsu, 1999)

$$g(t) = \left\{ \frac{20}{3}\frac{1}{t^2}\left[1-(1+t)\exp(-t)\right] - \frac{12}{3}\left[\frac{6}{t^4} - \left(\frac{6}{t^4}+\frac{6}{t^3}+\frac{3}{t^2}+\frac{1}{t}\right)\exp(-t)\right]\right\}. \tag{28}$$

The streamwise displacement variance is given by

$$\sigma^2_x(t) = 2\sigma^2_{w_x} \int_0^t dt' \int_0^{t'} dt'' \rho_{w_x}(t''). \tag{29}$$

Explicit evaluation of the double integral using expression (28) gives (Dagan, 1988)

$$\sigma^2_x(t) = \sigma^2_Y \overline{v}\ell_Y \left[2t/\tau_v - 3\ln(t/\tau_v) + \frac{3}{2} - 3\gamma - E_1(t/\tau_v) + \frac{\tau_v^2\exp(-t/\tau_v)(1+t/\tau_v)-1}{t^2}\right]. \tag{30}$$

Figure 2 shows the evolution of $\sigma_x(t)$ from Eq. (30). Also here, the perturbation theory expression is a good quantitative descriptor for overall evolution of σ^2_x, but underestimates the numerical data at asymptotic times. In the following, we discuss a stochastic time-domain random walk model to describe solute dispersion for strong spatial heterogeneity.

3.2 Stochastic time-domain random walk

We use a stochastic time-domain random approach to quantify particle motion at large spatial heterogeneity. The time-domain random walk approach models particle motion at equidistant displacements along streamlines based on Equations (6). This approach

has been used to quantify streamwise particle transport, that is, arrival time distributions, streamwise concentration profiles and displacement moments in porous and fractured media (Painter et al., 2008; Kang et al., 2011; Comolli et al., 2019; Hyman et al., 2019). In the following, we briefly recapitulate the modeling of streamwise particle motion using the approach of Comolli et al. (2019), before we analyze the dynamics of transverse motion.

3.2.1 Streamwise motion

The streamwise motion of solute particles is described by the following set of equations (Dentz et al., 2016; Comolli et al., 2019),

$$\frac{dx(s)}{ds} = \chi^{-1}, \qquad \frac{dt(s)}{ds} = \frac{1}{v_s(s)}, \tag{31}$$

where χ denotes the advective tortuosity (Koponen et al., 1996), which is defined as

$$\chi = \frac{\overline{v}_e}{\overline{v}} = \frac{1}{\langle \cos[\alpha(s)] \rangle}, \tag{32}$$

The analysis of Hakoun et al. (2019) for two-dimensional Darcy-scale heterogeneous porous media showed that the series of equidistant particle speeds $\{v_s(s)\}$ can be modeled in terms of an Ornstein-Uhlenbeck process for the normal scores transform $\omega(s)$ of $v_s(s)$. The normal score transform is defined as

$$\omega(s) = \Phi^{-1}\{P_s[v(s)]\}, \tag{33}$$

where $\Phi(w)$ is the cumulative unit Gaussian distribution, and $\Phi^{-1}(s)$ its inverse, $P_s(v)$ is the cumulative distribution of $v_s(s)$. The normal score transform $\omega(s)$ satisfies

$$\frac{d\omega(s)}{ds} = -\frac{\omega(s)}{\ell_c} + \sqrt{\frac{2}{\ell_c}}\eta(s), \tag{34}$$

where ℓ_c denotes the correlation length, and $\eta(s)$ is a Gaussian white with zero mean and covariance $\langle \eta(s)\eta(s') \rangle = \delta(s - s')$. Hakoun et al. (2019) found the following empirical relationship between between ℓ_c and the statistics of the underlying hydraulic conductivity field (see also Table 1),

$$\ell_c = \ell_Y(0.181\sigma_Y^2 + 2.221). \tag{35}$$

This regression is consistent with the prediction $\ell_c = 8\ell_Y/3$ of perturbation theory (Cvetkovic et al., 1996).

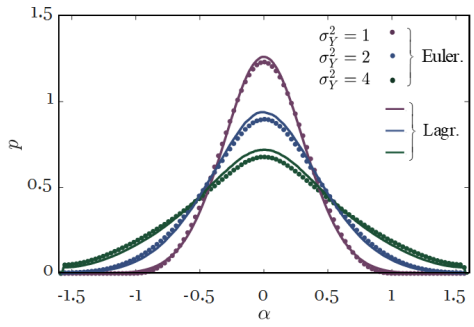

Figure 3: Probability distribution of the angle α obtained from (circles) spatial sampling and (solid lines) equidistant sampling along streamlines for $\sigma_Y^2 = (1, 2, 4)$.

3.2.2 Transverse motion

Here, we analyze transverse particle motion in order to understand and quantify its stochastic dynamics. The equation of motion of solute particles in direction transverse to the mean flow can be written as

$$\frac{d\hat{y}(s)}{ds} = \sin[\alpha(s)]. \tag{36}$$

In order to probe the transverse motion, we analyze the distribution of $\alpha(s)$ sampled along and across trajectories

$$p_\alpha(a) = \frac{1}{V_0}\int_{\Omega_0} d\mathbf{x}_0 \frac{1}{L}\int_0^L ds' \delta[a - \alpha(s', \mathbf{x}_0)], \tag{37}$$

where $\alpha(s, \mathbf{x}_0)$ denotes the angle along the trajectory that starts at $\mathbf{x}_0$, Ω_0 the set of initial points and V_0 its volume. We assume that the distribution is stationary, that is, it does not depend on s. We also consider sampling of the angle $\alpha(\mathbf{x})$ in space,

$$p'_\alpha(a) = \frac{1}{V}\int_\Omega d\mathbf{x}\delta[a - \alpha(\mathbf{x})]. \tag{38}$$

Figure 3 shows that the two sampling methods give approximately the same distribution, which indicates that the angle α is independent from the velocity. This observation is consistent with the findings of Meyer et al. (2013).

The distribution $p_\alpha(a)$ has zero mean and is symmetric around zero. In fact, as shown in Section 3.1, perturbation theory indicates that for low degree of heterogeneity $\alpha(s)$ is Gaussian distributed with variance $\sigma_\alpha^2 = \sigma_Y^2/8$. Figure 4a suggests that for increasing disorder, $p_\alpha(a)$ follows a Gaussian distribution that is wrapped around the unit cir-

cle, i.e., a wrapped Gaussian distribution (Fisher, 1993). In Figure 4, data for the angle distribution is compared with the wrapped Gaussian distribution. While perturbation theory provides a good estimate for the shape of $p_\alpha(x)$, it overestimates the width of $p_\alpha(a)$ for increasing σ_Y^2. Thus, we adjust σ_α^2 on the base of the Eulerian statistics of the angle α, see previous discussion of Figure 3.

Furthermore, we consider the Lagrangian correlation function of $\alpha(s)$, which is defined by

$$\rho_\alpha(s) = \frac{1}{\sigma_\alpha^2 V_0} \int_{\Omega_0} d\mathbf{x}_0 \frac{1}{L} \int_0^L ds' \alpha(s+s', \mathbf{x}_0)\alpha(s', \mathbf{x}_0). \tag{39}$$

Again, we assume that the statistics are stationary. As shown in Section 3.1, perturbation theory indicates that $\rho_\alpha(s)$ is indeed stationary and given by $\rho_\alpha(s) = f(s/\ell_Y)$, where $f(s)$ is given by (19). Figure 4b shows $\rho_\alpha(s)$ for different σ_Y^2. The correlation decays sharply at short distances and becomes negative for distances larger than ℓ_Y, that is, at larger distances, angles are persistently anti-correlated. Note that, expression (19) embeds these features while there is a quantitative mismatch with the numerical data. Thus, for increasing σ_Y^2, we represent the correlation function by Eq. (19) as

$$\rho_\alpha(s) = f(s/\ell_a), \tag{40}$$

where the correlation length ℓ_a is adjusted from the tail of the empirical Lagrangian correlation function to capture the long-range anti-correlation. Based on these observations, in the following, we first pose a Markov model for the evolution of the angle, and then a long-range correlated model.

3.2.2.1 Ornstein-Uhlenbeck process Based on the observation that the correlation function $\rho_\alpha(s)$ decays rapidly to zero with lag-distance s, and that its distribution is Gaussian, we pose an Ornstein-Uhlenbeck process for $\alpha(s)$ that has both these properties. Thus, the angle follows the Langevin equation

$$\frac{d\alpha(s)}{ds} = -\frac{\alpha(s)}{\ell_\alpha} + \sqrt{2\frac{\sigma_\alpha^2}{\ell_\alpha}}\eta(s), \tag{41}$$

where ℓ_α denotes a characteristic fluctuation scale of $\alpha(s)$. In this approach, the correlation function $\rho_\alpha(s)$ is exponential (Gardiner, 1986),

$$\rho_\alpha(s) = \exp(-|s|/\ell_\alpha). \tag{42}$$

In order to asses the validity of this approach, we compare it to the perturbation theory results for the displacement variance $\hat{\sigma}_y^2(s)$ for $s \gg \ell$. Equation (24) indicates

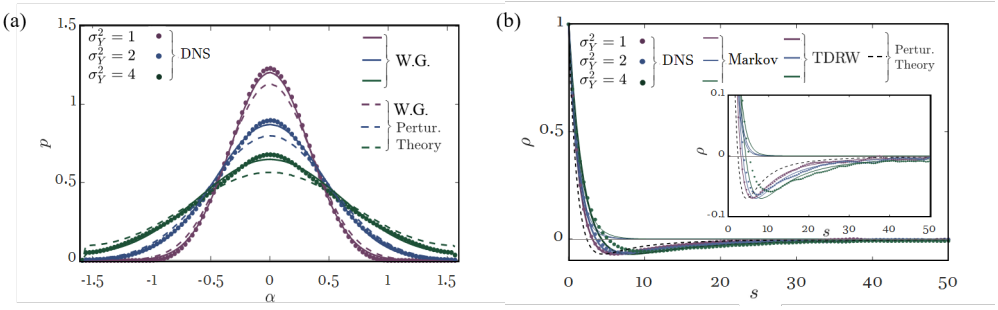

Figure 4: (a) Probability distribution of $\alpha(s)$ grounded on (circles) the DNS, wrapped Gaussian distributions with σ_α^2 parameterized by (dashed lines) perturbation theory and (solid lines) by the Eulerian statistics of α, for $\sigma_Y^2 = (1, 2, 4)$. (b) Correlation function of $\alpha(s)$ from (circles) DNS, (thin solid lines) a Markov model, (black dashed line) perturbation theory, and (thick solid lines) perturbation theory with adjusted correlation length ℓ_a.

that $\hat{\sigma}_y^2(s) \sim \ln(s/\ell_Y)$ increases with the logarithm of distance s. For weak heterogeneity, that is, $\sigma_\alpha^2 \ll 1$, the transverse displacement can be approximated by

$$\frac{d\hat{y}(s)}{ds} = \alpha(s), \tag{43}$$

and the correlation length is $\ell_\alpha = \ell_Y$. Using expression (42) in Eq. (21) gives for $s \gg \ell_Y$

$$\hat{\sigma}_y^2(s) = 2\sigma_\alpha^2 \ell_Y s. \tag{44}$$

It increases linearly with distance. Thus, the asymptotic behavior of the Markov model (41) is not compatible with the true behavior at large distances. Thus, in the following, we consider a model that reproduces the large time behaviors predicted by perturbation theory.

3.2.2.2 Stationary correlated Gaussian process Careful inspection of $\rho_\alpha(s)$ in Figure 4b reveals that after the sharp initial decrease of the correlation function, a persistent degree of anti-correlation emerges. The latter is a fundamental aspect of transverse motion, and is a consequence of the solenoidal character of the flow field, that is, $\nabla \cdot \mathbf{q}(\mathbf{x}) = 0$. This property leads to the meandering of the streamlines as shown in Figure 1.

It is important to note that the negative values of $\rho_\alpha(s)$ are small. That is, while particles tend to persistently change the transverse direction, the magnitudes of the trans-

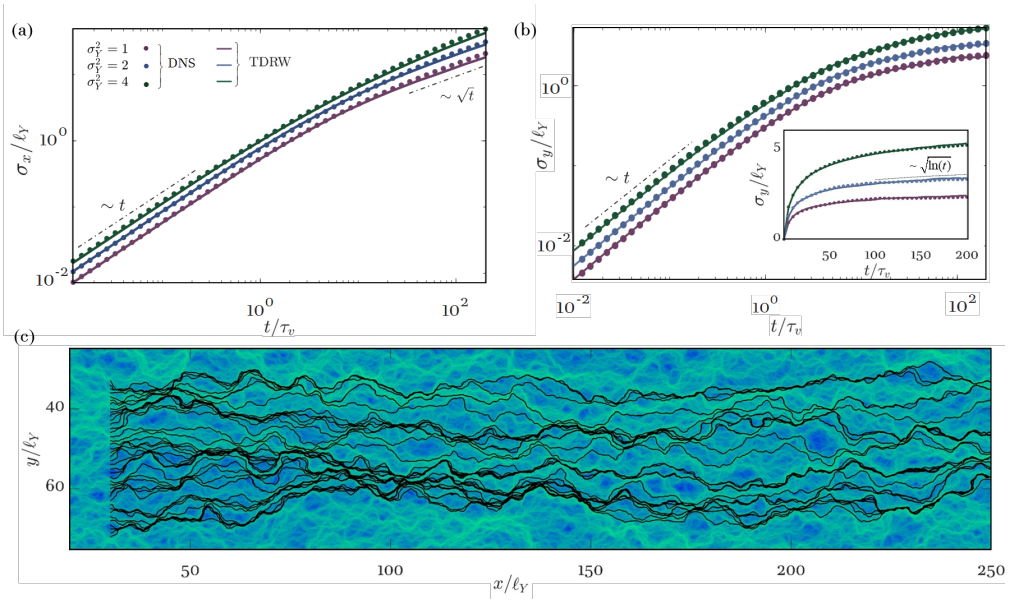

Figure 5: Time behaviour of (a) the longitudinal σ_x and (b) the transverse σ_y (inset bilinear scale) dispersion scales for $\sigma_Y^2 = (1, 2, 4)$. (c) Samples of particle trajectories (black curves) released in a Darcy' flow field (v, logarithmic scale, blue low and green high) for $\sigma_Y^2 = 4$: focusing of the trajectories in the nearest set of preferential flow paths underpins the intense growth of $\sigma_y(t)$ at middle times ($\mathcal{O}(t) \sim (1 - 10)\tau_v$), while the meandering of the trajectories sustains the logarithmic growth of $\sigma_y(t)$ at the large scale ($\mathcal{O}(t) \sim 100\tau_v$).

verse excursions are only weakly correlated. In other words, the asymmetry of $\rho_\alpha(s)$ in terms of streamwise persistence and intensity of the anti-correlation are the key elements underpinning the limitation of particle motion in the transverse direction that manifests ultraslow transverse dispersion as expressed by Eq. (24). As shown in Section 3.1, perturbation theory indicates that the angle process $\alpha(s)$ can be described as a stationary correlated Gaussian noise. In full analogy, for large disorder variance we also model $\alpha(s)$ as a correlated Gaussian process characterized by the correlation function (40).

To generate trajectories of $\alpha(s)$, it is convenient to introduce the covariance function of α, which is definded by $C_\alpha(s) = \sigma_\alpha^2 \rho_\alpha(s)$. The covariance function can be expanded as

$$C_\alpha(s) = \sum_{n=1}^{\infty} \lambda_n \phi_n(s), \tag{45}$$

σ_Y^2	χ	σ_α^2	ℓ_c	ℓ_α
1	1.06	0.11	2.4	1.28
2	1.1	0.21	2.58	1.4
4	1.2	0.38	2.95	1.8

Table 1: Values of model parameters in the two-dimensional stochastic time-domain random walk approach.

where the $\phi_n(s)$ are the eigenfunctions and the λ_n the respective eigenvalues of $C_\alpha(s)$ (D. Zhang & Lu, 2004; Dell'Oca & Porta, 2020). Thus the stochastic process $\alpha(s)$ can be represented by the Karhunen-Loève expansion

$$\alpha(s) = \sum_{n=1}^{\infty} \sqrt{\lambda_n}\phi_n(s)\xi_n, \tag{46}$$

where the ξ_n are independent identically distributed Gaussian random variables of zero mean and unit variance. The numerical implementation is detailed in Appendix A.

4 Transport behaviors

In this section we compare the predictions of the stochastic time domain random walk model with data from direct numerical simulations for the longitudinal and transverse dispersive scales, streamwise and transverse particle distribution, as well as the full two-dimensional particle distributions. The direct flow and transport simulations are described in Section 2.3. We consider media characterized by $\sigma_Y^2 = (1, 2, 4)$.

The model parameters χ and σ_α^2 of the stochastic time-domain random walk model are fully constrained by the Eulerian flow properties. The correlation legnth ℓ_c is given by the regression in Eq. (35). The correlation length ℓ_α is adjusted from the Lagrangian correlation function as outlined in Section 3.2.2. Table 1 lists the values of ℓ_c, χ, σ_α^2 and ℓ_α for the different values of σ_Y^2.

4.1 Spatial variance

Figure 5 shows the time behaviour of the streamwise and transverse dispersion scales σ_x and σ_y from the the direct numerical simulations and the stochastic time-domain random walk model. In agreement with Comolli et al. (2019), the stochastic TDRW describes

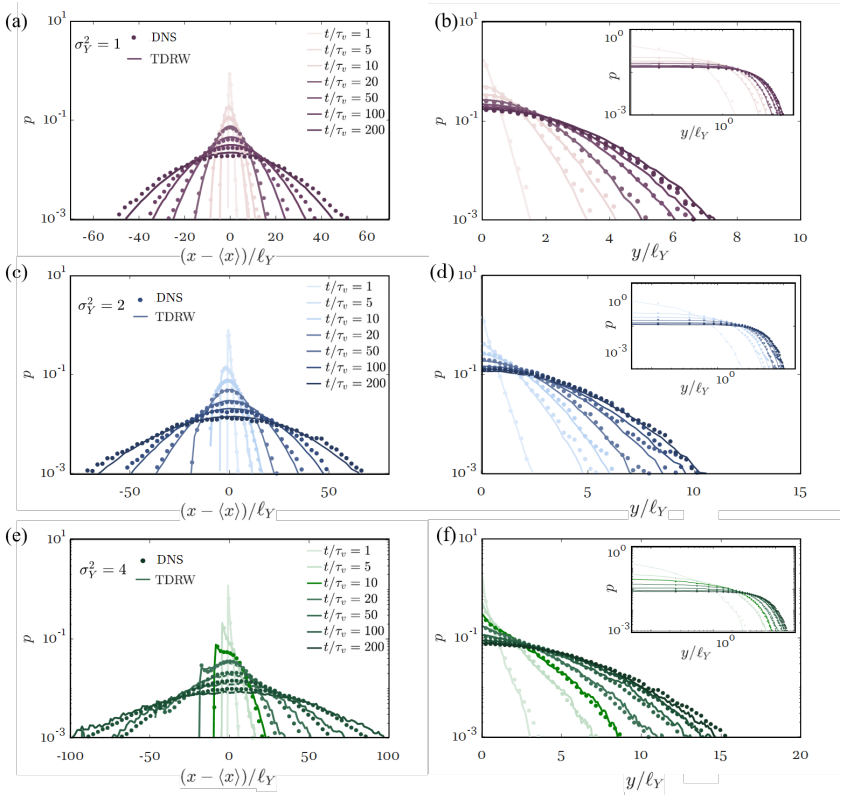

Figure 6: Probability distribution of particle position along the longitudinal, i.e., $p(x,t)$, and transverse, i.e., $p(y,t)$ (only the positive branch of the symmetric distribution is depicted), directions at diverse times considering (a, d) $\sigma_Y^2 = 1$, (b, e) $\sigma_Y^2 = 2$ and (c, f) $\sigma_Y^2 = 4$. Results based on the (symbols) direct numerical simulations and (solid lines) TDRW are depicted.

the full temporal evolution of σ_x including the ballistic regimes for $t < \tau_v$, in which $\sigma_x(t) \sim t$, and the cross-over from ballistic to the asymptotic behaviors $\sigma_x \sim \sqrt{t}$ at times $t \gg \tau_v$.

The stochastic TDRW model captures also the full time evolution of $\sigma_y(t)$ including the early time ballistic regime and the transition to ultraslow diffusion at times $t \gg \tau_v$. The strong increase of σ_y at intermediate times reflects the focusing of solute particles from their initial positions into flow channels as illustrated in Figure 5c. For later times, the transverse displacement is determined by the meandering of these flow channels, see Figures 1 and 5c. This meandering confines transverse motion at large-scale, which is here qualitatively and quantitatively reproduced by the stochastic TDRW model.

4.2 Particle distributions

In addition to the dispersion scales, we consider now the longitudinal and transverse particles distributions. Figure 6 depicts snapshots of $p(x,t)$ and $p(y,t)$ at different times. For $p(y,t)$ only the positive branch of the symmetric distribution is shown.

Figures 6a, c, and e show satisfactory agreement between the numerical data for $p(x,t)$ and the stochastic TDRW model, which is able to reproduce the full transition from initially skewed to asymptotic Gaussian behavior for moderately to strongly heterogeneous media.

Figures 6b, d, and f highlights the satisfactory agreement between the numerical data for $p(y,t)$ and the stochastic TDRW model from early to late times, and for all degrees of heterogeneity under consideration. We observe a rapid expansion of $p(y,t)$ at the early times (e.g., $t = (1,5,10)\tau_v$), that is, as the solute particles tend to be focused towards the nearest flow channels such that larger absolute values of y become more likely. As time passes ($t = (20,50,100,200)\tau_v$), solute particles travel within flow channels characterized by a meandering structure which underpins the decreasing rate of expansion of $p(y,t)$, consistent with the behavior of $\sigma_y(t)$ shown in Figure 5. Note that, $p(y,t)$ tends toward Gaussianity at late times (e.g., $t = (100,200)\tau_v$). Gotovac et al. (2009) considered the transverse particle distribution after fixed travel distances and found that it approaches Gaussianity already after relatively short distances of about $5\ell_Y$. Our results for the distribution of $\hat{y}(s)$ after fixed travel distances s (not shown) confirm these findings.

Finally, we consider the joint distribution $p(\mathbf{x},t)$ of streamwise and transverse particle positions at different times. Figure 7 depicts $p(\mathbf{x},t)$ from the numerical data in the upper half of each panel, and the stochastic TDRW model in the lower half, at times $t = (5,20,50)\tau_v$ for $\sigma_Y^2 = 1,2,4$. We find an overall satisfactory agreement between the numerical data and the stochastic TDRW model, which corroborates the assumption of treating the streamwise longitudinal and transverse transport as two independent stochastic processes (Meyer et al., 2013; Meyer & Tchelepi, 2010).

5 Conclusions

We analyze the stochastic dynamics of two-dimensional particle motion in Darcy-scale heterogeneous porous media. The spatial variability of the hydraulic conductivity

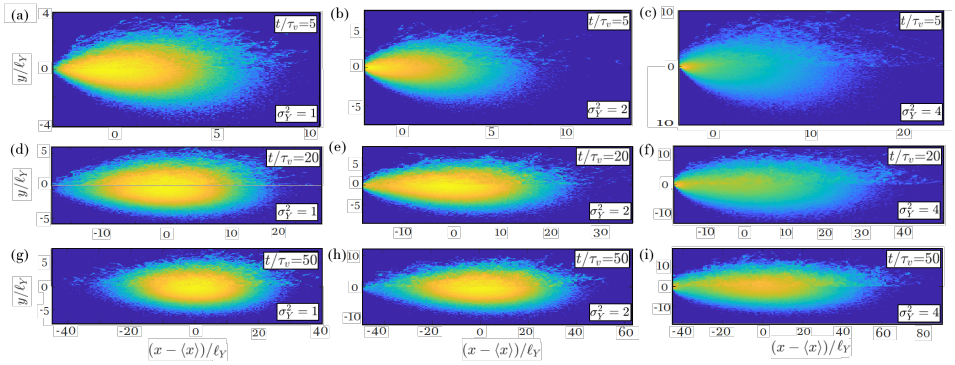

Figure 7: Joint probability distribution of particles locations $p(\mathbf{x}, t)$ at times $t = (5, 20, 50)$ and for diverse degree of formation heterogeneity (a, d, g) $\sigma_Y^2 = 1$, (b, e, h) $\sigma_Y^2 = 2$ and (c, f, i) $\sigma_Y^2 = 4$. Results grounded on the DNS and on the stochastic model are depicted in the top and bottom half of each panel, respectively. The colormap is in logarithmic scale (blue low, yellow high).

is represented using a stochastic modeling approach such the $K(\mathbf{x})$ is a realization of a lognormally distributed multi-Gaussian spatial random field. The Lagrangian particle dynamics are analyzed through numerical particle tracking simulations as well as perturbation theory by using an equidistant sampling strategy, which acknowledges the spatial organization of the Eulerian and Lagrangian flow velocities on a characteristic length scale. The perturbation theory analysis reveals that longitudinal particle motion is determined by the variability of travel times along streamlines, while transverse motion is determined by the fluctuation structure of transverse displacements. The former can be captured by a Markov model for the equidistantly sampled flow speeds, that is, flow speeds are only weakly correlated. The latter, however, turns out to be persistently anti-correlated as a consequence of the solenoidal character of the flow field. This strong anticorrelation leads to an ultraslow growth of the transverse displacement variance with distance and time. The transverse displacements are characterized by the series of angles between the streamlines and the mean flow direction. Perturbation theory shows that the angle distribution can be represented by a wrapped Gaussian distribution, which is valid also for increasing heterogeneity strength. Unlike the speed series, the angle series cannot be represented as a Markov process. The angular increments are modeled as a correlated Gaussian noise, which renders the angle process as a correlated Brownian motion. The

Gaussian increment process is generated here using a Karhunen-Loeve expansion. For low medium heterogeneity, the model can be fully constrained by medium and flow properties using perturbation theory. For increasing heterogeneity, the model can be constrained by Eulerian flow statistics and the characteristic length scale of the fluctuations of the Lagrangian angular series.

The proposed stochastic TDRW model combines a Markov model for the particle speeds with a correlated Gaussian noise for transverse particle displacements. Comparison with detailed numerical simulations for the longitudinal and transverse dispersion scales and the full particle distributions shows that the model captures the dynamics of advective particle motion both qualitatively and quantitatively. This underpins the critical importance of correctly representing the topological constraints of the underlying Eulerian flow field in the large scale particle dynamics (Lester et al., 2021, 2022). These behaviors cannot be accounted for by two-dimensional TDRW or CTRW schemes that model transverse displacements as Markov processes. The proposed stochastic TDRW model is able to quantify large scale longitudinal and transverse advective particle motion in two-dimensional divergence-free Darcy flows as can occur on shallow and stratified aquifers as well as rough fractures. The stochastic TDRW approach can be extended to flow and transport in three-dimensional porous media by following the same strategy as proposed in this paper.

6 Data Availability Statement

The computational data and codes for data analysis supporting this work are available upon request and as a Mendely Data repository at doi:10.17632/2bkc7gp2sd.2

Acknowledgments

We acknowledge funding from the European Union's Horizon 2020 research and innovation programme under the H2020-MSCA-IF-2019 scheme with the grant agreement No. 895152 (MixUQ). M.D. acknowledges the support of the Spanish Research Agency (10.13039/501100011033), Spanish Ministry of Science and Innovation through grants CEX2018-000794-S and HydroPore PID2019-106887GB-C31. A.D. gratefully acknowledges P. Ackerer for sharing the numerical code for the flow problem.

Appendix A Generation of long-range correlated stochastic angle series

The eigenvalues λ_n and eigenfunctions $\phi_n(s)$ of the covariance function $C_\alpha(s)$ are obtained from the following Fredholm equation

$$\int_0^\infty C_\alpha(s-s')\phi_n(s')ds' = \lambda_n\phi_n(s). \tag{A1}$$

For general $C_\alpha(s)$, Eq. (A1) can be solved numerically as outlined in the following. Firstly, we discretize s into N intervals of length Δs such that $s_i = i\Delta s$. Then, we define the symmetric $N \times N$ covariance matrix C_{ij} as

$$C_{ij} = C_\alpha(s_i - s_j)\Delta s. \tag{A2}$$

The eigenfunctions are discretized as $\phi_i^{(n)} = \phi_n(s_i)$ and are represented by the eigenvectors $\boldsymbol{\phi}^{(n)}$. Teh angle process is discretized as $\alpha_i = \alpha(s_i)$ and represented by the vector $\boldsymbol{\alpha}$.

The discrete version of Eq. (A1) is

$$\mathbf{C}\boldsymbol{\phi}^{(n)} = \lambda_n\boldsymbol{\phi}^{(n)}. \tag{A3}$$

The eigenvalues of $\mathbf{C}$ are obtained from

$$\det\left(\mathbf{C} - \lambda\mathbb{I}\right) = 0, \tag{A4}$$

where $\mathbb{I}$ is the identity matrix. The eigenvector $\boldsymbol{\phi}^{(n)}$ corresponding to the nth eigenvalue λ_n is obtained by solving Eq. (A3). Thus realizations of the correlated Gaussian process $\boldsymbol{\alpha}$ are generated according to the discrete version of Eq. (46) as

$$\boldsymbol{\alpha} = \sum_{n=1}^{N_\lambda} \sqrt{\lambda_n}\boldsymbol{\phi}^{(n)}\xi_n. \tag{A5}$$

Here we set $N_\lambda = 1000 < N$ modes. Furthermore, we set $\Delta s = l_Y/10$ and $N = 5000$. The computation of the eigenvalues and eigenvectors is carried out with standard commands in MATLAB (MathWorks, 2015).

References

Abramowitz, M., & Stegun, I. A. (1972). *Handbook of mathematical functions.* Dover Publications, New York.

Attinger, S., Dentz, M., & Kinzelbach, W. (2004). Exact transverse macro dispersion coefficients for transport in heterogeneous porous media. *Stochastic Environ-*

mental Research and Risk Assessment, *18*(1), 9-15. doi: https://doi.org/10.1007/s00477-003-0160-6

Bear, J. (1972). *Dynamics of fluids in porous media*. American Elsevier, New York.

Bellin, A., Salandin, P., & Rinaldo, A. (1992). Simulation of dispersion in heterogeneous porous formations: Statistics, first-order theories, convergence of computations. *Water Resources Research*, *28*(9), 2211–2227.

Bénichou, O., & Oshanin, G. (2002). Ultraslow vacancy-mediated tracer diffusion in two dimensions: The einstein relation verified. *Phys. Rev. E*, *66*, 031101.

Benson, D. A., Wheatcraft, S. W., & Meerschaert, M. M. (2000). Application of a fractional advection-dispersion equation. *Water resources research*, *36*(6), 1403–1412.

Berkowitz, B., Cortis, A., Dentz, M., & Scher, H. (2006). Modeling non-fickian transport in geological formations as a continuous time random walk. *Reviews of Geophysics*, *44*(2).

Bijeljic, B., Mostaghimi, P., & Blunt, M. J. (2011). Signature of non-fickian solute transport in complex heterogeneous porous media. *Physical review letters*, *107*(20), 204502.

Boettcher, S., & Sibani, P. (2011). Ageing in dense colloids as diffusion in the logarithm of time. *Journal of Physics: Condensed Matter*, *23*(6), 065103.

Comolli, A., Hakoun, V., & Dentz, M. (2019). Mechanisms, upscaling, and prediction of anomalous dispersion in heterogeneous porous media. *Water Resources Research*, *55*(10), 8197–8222.

Cvetkovic, V., Cheng, H., & Wen, X. H. (1996). Analysis of nonlinear effects on tracer migration in heterogeneous aquifers using lagrangian travel time statistics. *Water Resources Research*, *32*(6), 1671-1680.

Cvetkovic, V., Fiori, A., & Dagan, G. (2014). Solute transport in aquifers of arbitrary variability: A time-domain random walk formulation. *Water Resources Research*, *50*(7), 5759–5773.

Dagan, G. (1984). Solute transport in heterogeneous porous formations. *Journal of Fluid Mechanics*, *145*, 151–177. doi: 10.1017/S0022112084002858

Dagan, G. (1988). Time-dependent macrodispersion for solute transport in anisotropic heterogeneous aquifers. *Water Resources Research*, *24*(9), 1491-1500. Retrieved from `https://agupubs.onlinelibrary.wiley.com/doi/abs/10.1029/`

WR024i009p01491 doi: https://doi.org/10.1029/WR024i009p01491

Dagan, G. (1989). *Flow and transport in porous formations.* Springer, New York.

de Dreuzy, J.-R., Beaudoin, A., & Erhel, J. (2007). Asymptotic dispersion in 2d heterogeneous porous media determined by parallel numerical simulations. *Water Resources Research*, *43*(10).

Dell'Oca, A., & Porta, G. M. (2020). Characterization of flow through random media via karhunen–loève expansion: an information theory perspective. *GEM-International Journal on Geomathematics*, *11*(1), 1–18.

Dell'Oca, A., Riva, M., Ackerer, P., & Guadagnini, A. (2019). Solute transport in random composite media with uncertain dispersivities. *Advances in Water Resources*, *128*, 48–58.

Dell'Oca, A., Riva, M., Carrera, J., & Guadagnini, A. (2018). Solute dispersion for stable density-driven flow in randomly heterogeneous porous media. *Advances in Water Resources*, *111*, 329–345.

Dentz, M., & Castro, A. (2009). Effective transport dynamics in porous media with heterogeneous retardation properties. *Geophys. Res. Lett.*, *36*, L03403.

Dentz, M., Comolli, A., Hakoun, V., & Hidalgo, J. J. (2020). Transport upscaling in highly heterogeneous aquifers and the prediction of tracer dispersion at the made site. *Geophysical Research Letters*, *47*(22), e2020GL088292.

Dentz, M., Cortis, A., Scher, H., & Berkowitz, B. (2004). Time behavior of solute transport in heterogeneous media: transition from anomalous to normal transport. *Advances in Water Resources*, *27*(2), 155–173.

Dentz, M., Hidalgo, J. J., & Lester, D. (2022). Mixing in porous media: Concepts and approaches across scales. *Transport in Porous Media*, 1–49.

Dentz, M., Kang, P. K., Comolli, A., Le Borgne, T., & Lester, D. R. (2016). Continuous time random walks for the evolution of lagrangian velocities. *Physical Review Fluids*, *1*(7), 074004.

Deutsch, C. V., & Journel, A. G. (1992). *Gslib: Geostatistical software library and user's guide.* Oxford University Press, New York, NY.

Domenico, P. A., & Schwartz, F. W. (1998). *Physical and chemical hydrogeology* (Vol. 506). Wiley New York.

Edery, Y., Guadagnini, A., Scher, H., & Berkowitz, B. (2014). Origins of anomalous transport in heterogeneous media: Structural and dynamic controls. *Water*

Resources Research, *50*(2), 1490–1505.

Fiori, A., Dagan, G., Jankovic, I., & Zarlenga, A. (2013). The plume spreading in the made transport experiment: Could it be predicted by stochastic models? *Water Resources Research*, *49*(5), 2497–2507.

Fiori, A., Zarlenga, A., Gotovac, H., Jankovic, I., Volpi, E., Cvetkovic, V., & Dagan, G. (2015). Advective transport in heterogeneous aquifers: Are proxy models predictive? *Water resources research*, *51*(12), 9577–9594.

Fisher, N. I. (1993, October). *Statistical Analysis of Circular Data.* Retrieved 2023-03-17, from `https://www.cambridge.org/core/books/statistical-analysis-of-circular-data/324A46F3941A5CD641ED0B0910B2C33F` (ISBN: 9780521350181 9780521568906 9780511564345 Publisher: Cambridge University Press) doi: 10.1017/CBO9780511564345

Frippiat, C. C., & Holeyman, A. E. (2008). A comparative review of upscaling methods for solute transport in heterogeneous porous media. *Journal of Hydrology*, *362*(1-2), 150–176.

Gardiner, C. W. (1986). Handbook of stochastic methods for physics, chemistry and the natural sciences. *Applied Optics*, *25*, 3145.

Gotovac, H., Cvetkovic, V., & Andricevic, R. (2009). Flow and travel time statistics in highly heterogeneous porous media. *Water Resources Research*, *45*(7).

Haggerty, R., & Gorelick, S. M. (1995). Multiple-rate mass transfer for modeling diffusion and surface reactions in media with pore-scale heterogeneity. *Water Resour. Res.*, *31*, 2383–2400.

Hakoun, V., Comolli, A., & Dentz, M. (2019). Upscaling and prediction of lagrangian velocity dynamics in heterogeneous porous media. *Water Resources Research*, *55*(5), 3976–3996.

Harvey, C., & Gorelick, S. M. (2000). Rate-limited mass transfer or macrodispersion: Which dominates plume evolution at the macrodispersion experiment (made) site? *Water Resources Research*, *36*(3), 637-650. Retrieved from `https://agupubs.onlinelibrary.wiley.com/doi/abs/10.1029/1999WR900247` doi: https://doi.org/10.1029/1999WR900247

Havlin, S., & Ben-Avraham, D. (2002). Diffusion in disordered media. *Advances in Physics*, *51*(1), 187-292.

Hsu, K.-C. (1999). A general method for obtaining analytical expressions for the

first-order velocity covariance in heterogeneous porous media. *Water Resources Research*, *35*(7), 2273-2277. Retrieved from https://agupubs.onlinelibrary.wiley.com/doi/abs/10.1029/1999WR900117 doi: https://doi.org/10.1029/1999WR900117

Hu, Y., Xu, W., Zhan, L., Ye, Z., & Chen, Y. (2020). Non-fickian solute transport in rough-walled fractures: The effect of contact area. *Water*, *12*(7). Retrieved from https://www.mdpi.com/2073-4441/12/7/2049 doi: 10.3390/w12072049

Hyman, J. D., Dentz, M., Hagberg, A., & Kang, P. K. (2019, jan). Linking structural and transport properties in three-dimensional fracture networks. *Journal of Geophysical Research: Solid Earth*. Retrieved from https://doi.org/10.1029/2018jb016553 doi: 10.1029/2018jb016553

Kang, P. K., Dentz, M., Le Borgne, T., & Juanes, R. (2011). Spatial markov model of anomalous transport through random lattice networks. *Phys. Rev. Lett.*, *107*, 180602.

Kong, B., & Chen, S. (2018). Numerical simulation of fluid flow and sensitivity analysis in rough-wall fractures. *Journal of Petroleum Science and Engineering*, *168*, 546–561.

Koponen, A., Kataja, M., & Timonen, J. (1996). Tortuous flow in porous media. *Physical Review E*, *54*(1), 406.

Kottwitz, M. O., Popov, A. A., Baumann, T. S., & Kaus, B. J. (2020). The hydraulic efficiency of single fractures: correcting the cubic law parameterization for self-affine surface roughness and fracture closure. *Solid Earth*, *11*(3), 947–957.

Lester, D. R., Dentz, M., Bandopadhyay, A., & Le Borgne, T. (2021). The lagrangian kinematics of three-dimensional darcy flow. *Journal of Fluid Mechanics*, *918*.

Lester, D. R., Dentz, M., Bandopadhyay, A., & Le Borgne, T. (2022). Fluid deformation in isotropic darcy flow. *Journal of Fluid Mechanics*, *945*, A18.

MathWorks. (2015). *Matlab version: 8.6.0 (r2015b)*. Natick, Massachusetts, United States: The MathWorks Inc. Retrieved from https://www.mathworks.com

Meerschaert, M. M., Benson, D. A., & Baeumer, B. (2001). Operator lévy motion and multiscaling anomalous diffusion. *Phys. Rev. E*, *63*, 021112.

Meyer, D. W. (2017). Relating recent random walk models with classical perturbation theory for dispersion predictions in the heterogeneous porous subsurface. *Ad-*

vances in Water Resources, *105*, 227–232.

Meyer, D. W. (2018). A simple velocity random-walk model for macrodispersion in mildly to highly heterogeneous subsurface formations. *Advances in Water Resources*, *121*, 57–67.

Meyer, D. W., & Tchelepi, H. A. (2010). Particle-based transport model with markovian velocity processes for tracer dispersion in highly heterogeneous porous media. *Water Resources Research*, *46*(11).

Meyer, D. W., Tchelepi, H. A., & Jenny, P. (2013). A fast simulation method for uncertainty quantification of subsurface flow and transport. *Water Resources Research*, *49*(5), 2359–2379.

Neuman, S. P., & Tartakovsky, D. M. (2009). Perspective on theories of non-fickian transport in heterogeneous media. *Advances in Water Resources*, *32*(5), 670–680.

Niemi, A., Bear, J., Bensabat, J., et al. (2017). *Geological storage of co2 in deep saline formations* (Vol. 29). Springer.

Painter, S. L., Cvetkovic, V., & Pensado, O. (2008). Time-domain random-walk algorithms for simulating radionuclide transport in fractured porous rock. *Nuclear Technology*, *163*(1), 129–136.

Pollock, D. (1988). Semianalytical computation of path lines for finite-difference models. *Ground Water*, *26 (6)*, 743-750.

Rubin, Y. (2003). *Applied stochastic hydrogeology*. Oxford University Press.

Salandin, P., & Fiorotto, V. (1998). Solute transport in highly heterogeneous aquifers. *Water Resources Research*, *34*(5), 949-961. Retrieved from `https://agupubs.onlinelibrary.wiley.com/doi/abs/10.1029/98WR00219` doi: https://doi.org/10.1029/98WR00219

Song, C., Koren, T., Wang, P., & Barabási, A.-L. (2010). Modelling the scaling properties of human mobility. *Nature Physics*, *6*, 818–823.

Sperl, M. (2005). Nearly logarithmic decay in the colloidal hard-sphere system. *Phys. Rev. E*, *71*, 060401.

Wang, W., & Barkai, E. (2020). Fractional advection-diffusion-asymmetry equation. *Phys. Rev. Lett.*, *125*, 240606. Retrieved from `https://link.aps.org/doi/10.1103/PhysRevLett.125.240606` doi: 10.1103/PhysRevLett.125.240606

Wang, Z., Xu, C., Dowd, P., Xiong, F., & Wang, H. (2020). A nonlinear version of the reynolds equation for flow in rock fractures with complex void geometries.

Water Resources Research, *56*(2), e2019WR026149.

Younes, A., Ackerer, P., & Delay, F. (2010). Mixed finite elements for solving 2-d diffusion-type equations. *Reviews of Geophysics*, *48*(1).

Zhang, D., & Lu, Z. (2004). An efficient, high-order perturbation approach for flow in random porous media via karhunen–loeve and polynomial expansions. *Journal of Computational Physics*, *194*(2), 773–794.

Zhang, Y., & Benson, D. A. (2013). Lagrangian simulation of multidimensional anomalous transport at the made site. *Geophysical Research Letters*, *35*(7).

Zhang, Y., Benson, D. A., & Reeves, D. M. (2009). Time and space nonlocalities underlying fractional-derivative models: Distinction and literature review of field applications. *Advances in Water Resources*, *32*(4), 561–581.

Zimmerman, R. W., & Bodvarsson, G. S. (1996). Hydraulic conductivity of rock fractures. *Transport Porous Med.*, *23*(1), 1–30.